Numerical Simulation of Nonadiabatic Electron Excitation in the Strong Field Regime. 2. Linear Polyene Cations

Stanley M. Smith,[†] Xiaosong Li,[‡] Alexei N. Markevitch,[§,||] Dmitri A. Romanov,[||,⊥] Robert J. Levis,[§,||] and H. Bernhard Schlegel*,[†]

Department of Chemistry, Wayne State University, Detroit, Michigan 48202, Department of Chemistry, University of Washington, Seattle, Washington 98195, and Departments of Chemistry and of Physics and Center for Advanced Photonics Research, Temple University, Philadelphia, Pennsylvania 19122

Received: July 6, 2005; In Final Form: September 29, 2005

Time-dependent Hartree−Fock theory has been used to study the electronic optical response of a series of linear polyene cations (+1 and +2) in strong laser fields. The interaction of ethylene, butadiene, and hexatriene, with pulsed and CW fields corresponding to 8.75×10^{13} W/cm^2 and 760 nm, have been calculated using the 6-31G(d,p) basis set. Nonadiabatic processes including nonlinear response of the dipole moment to the field and nonresonsnat energy deposition into excited states were more pronounced for the monocations in comparison with dications. For a given charge state and geometry, the nonadiabatic effects in the charge distribution and instantaneous dipole increased with the length of the polyene. For pulsed fields, the instantaneous dipole continued to oscillate after the field returned to zero and corresponded to a nonresonant electronic excitation involving primarily the lowest electronic transition. For a given molecule and fixed charge state, the degree of nonadiabatic coupling and excitation was greater for geometries with lower excitation energies.

I. Introduction

Understanding the electronic and nuclear dynamics of polyatomic molecules subjected to intense laser fields is central to unraveling many recent coherent control demonstrations.[1,2] Intense laser fields cause a variety of nonperturbative phenomenon that are typically called strong field effects. Some of these phenomena include field tunneling and barrier suppression ionization,[3−6] above threshold ionization (ATI),[7−9] higher-order harmonic generation,[10−14] and nonadiabatic multielectron dynamics (NMED).[15−18] Each process requires an understanding of the electronic response to the strong laser field. Incorporation of coupled electron−nuclear motion is necessary to understand phenomena such as above-threshold dissociation,[8,19] bond softening and hardening,[8,19,20] charge-resonance enhanced ionization,[21,22] Coulomb explosions,[22−25] and nonadiabatic charge localization. Understanding the response of the electronic wave function to strong fields is essential for the description of these phenomena, particularly in polyatomic molecules.

Intense laser dissociation and ionization processes have been reported for conjugated polyatomic molecules such as benzene, naphthalene, anthracene, hexatriene, octatetraene, decatetraene, and C_{60}.[3,15−18,26−30] In the low field limit, the response of the molecules to the laser field is mainly determined by transition dipole matrix elements and first-order polarizability. Nonlinear contributions arise from higher order polarizabilities. These properties have been extensively studied for linear polyenes[31−40] and their molecular cations.[38,41] At high intensities, electrons can be excited through multiphoton and nonadiabatic multielectron dynamical processes[15−18] such as Landau−Dykhne type excitations. A series of polyenes with increasing length exhibited increasing nonadiabatic coupling when subjected to a high intensity laser field.[42]

A wealth of information is available for excitation of H_2 in strong laser fields from calculations by Bandrauk et al. and others using wave packet dynamics.[21,43−47] Exact results have been reported for the H_2 intense laser field ionization which reveal that the structure of the ion significantly effects the ionization rate. The Parser−Parr−Pople (PPP) Hamiltonian has been used to simulate π electron dynamics[48] for octatetraene, and time-dependent Hartree−Fock methods have been used to model ionization saturation intensities in a multielectron system in a finite one-dimensional box.[49] Recently, we reported that time-dependent Hartree−Fock theory provides a good approximation to the electronic optical response of a series of linear polyenes in strong laser fields.[42] The response of several molecules, ethylene, butadiene, and hexatriene, was calculated with the 6-31G(d,p) basis set in the presence of a field corresponding to 8.75×10^{13} W/cm^2 with a wavelength of 760 nm. Time evolution of the electron population indicated that not only the π electrons but also lower lying valence electrons are involved in the electronic response. When the laser field is aligned with the long axis of the molecule, Löwdin population analysis revealed large charge buildup on the carbons at end of the molecule. For ethylene, the instantaneous dipole moment responded adiabatically to the applied the field, but for hexatriene, extensive nonadiabatic behavior was observed. At constant intensity, the nonadiabatic response in the charge distribution, instantaneous dipole, and orbital populations increased nonlinearly with the length of the polyene. These calculations have initiated clarification of the possible mechanisms of strong field nonadiabatic electron excitation leading to eventual molecular fragmentation.

There is building evidence that suggests conjugated molecules, including linear polyenes, ionize before dissociating. When a series of polyacenes (benzene, naphthalene, anthracene,

[†] Wayne State University.
[‡] University of Washington.
[§] Department of Chemistry, Temple University.
[||] Center for Advanced Photonics Research, Temple University.
[⊥] Department of Physics, Temple University.

10.1021/jp053696x CCC: $30.25
Published on Web 11/02/2005

and tetracene) was subjected to strong laser fields, both ionization and dissociation were observed.[17,18] The laser intensity for dissociation increases from approximately 1×10^{12} for tetracene to 1×10^{14} W/cm^2 for benzene at 760 nm. Below these intensities, molecular +1 cations are observed with little or no accompanying fragmentation. Except for benzene,[38] the calculated polarizability of each +1 cation in this series increases on ionization. Thus the laser field coupling increases upon single ionization, implying that fragmentation most probably proceeds on the cation surface. These results are not unique to the polyacenes. Similar experiments were performed on saturated and unsaturated linear hydrocarbons.[16,50,51] For a laser field intensity of 1×10^{14} W/cm^2 at ca. 800 nm, hexatriene +1 and +2 molecular ions are observed with little or no dissociation. Again, the calculated polarizability of the +1 molecular ion for hexatriene is larger than the polarizability of the neutral.[38] These results likewise suggest that dissociation may take place on the ion surface.

In the present work we use time-dependent Hartree−Fock theory to probe multielectron nonadiabatic processes in the +1 and +2 cations of linear conjugated hydrocarbons. Two limiting cases can be envisioned. First, the molecule could be subject to the strong field immediately upon ionization, and hence be close to the equilibrium geometry of the neutral. Alternatively, sufficient time could elapse so that the ionized system relaxes to its equilibrium geometry before the strong field is applied. These limiting cases are the subject of this paper. Between these limits, the dynamics of the molecule must be considered. The coupled electron−nuclear dynamics in the strong field regime will be the subject of future studies.[52]

Here we investigate photoinduced processes in molecules when $E_{max} = 0.05$ au and $\omega = 0.06$ au, corresponding to an intensity of 8.75×10^{13} W/cm^2 and 760 nm, which is identical to the conditions of our previous study. Because the electric field is applied for only a short time (~7 fs), significant ionization is not expected to occur during the laser pulse, and the chosen conditions allow us to discuss the observed trends as occurring prior to and after ionization. The nonresonant electronic response of these cations should range from adiabatic to nonadiabatic as observed for the neutral species.

II. Methodology

The time-dependent Hartree−Fock (TDHF) equations are typically used to describe the interactions of light with molecules.[45,53−58] The TDHF equations in an orthonormal basis can be written in terms of the Fock matrix, **F**, and the one-electron density matrix, **P**.

$$i\frac{d\mathbf{P}(t_i)}{dt} = [\mathbf{F}(t_i), \mathbf{P}(t_i)] \tag{1}$$

An efficient method for integrating the TDHF equations has been described in previous papers.[42,53] The Fock matrix depends on time not only because of the electric field of the laser, $\mathbf{E}(t)$, but also because of the time dependence of the electron density. Two temporal profiles were used for the laser field in the present TDHF simulations. For a continuous wave (CW) profile, the field envelope $|\mathbf{E}(t)|$ is ramped up linearly from zero to $|\mathbf{E}_{max}|$ at the end of the first cycle and thereafter remains at $|\mathbf{E}_{max}|$.

$$\begin{aligned} \mathbf{E}(t) &= (\omega t/2\pi)\mathbf{E}_{max} \quad \text{for} \quad 0 \le t \le 2\pi/\omega \\ \mathbf{E}_{max} &\quad \text{for} \quad t > 2\pi/\omega \end{aligned} \tag{2}$$

To simulate a short pulse, $|\mathbf{E}(t)|$ is increased linearly to $|\mathbf{E}_{max}|$ at the end of the first cycle, remains at $|\mathbf{E}_{max}|$ for one cycle, and then is decreased linearly to zero by the end of the next cycle.

$$\begin{aligned} \mathbf{E}(t) &= (\omega t/2\pi)\mathbf{E}_{max} \quad \text{for} \quad 0 \le t \le 2\pi/\omega \\ \mathbf{E}(t) &= \mathbf{E}_{max} \quad \text{for} \quad 2\pi/\omega \le t \le 4\pi/\omega \\ \mathbf{E}(t) &= (3 - \omega t/2\pi)\mathbf{E}_{max} \quad \text{for} \quad 4\pi/\omega \le t \le 6\pi/\omega \\ \mathbf{E}(t) &= 0 \quad \text{for} \quad t < 0 \text{ and } t > 6\pi/\omega \end{aligned} \tag{3}$$

The response of a molecule to an intense field can be characterized by several useful properties. The effective charge on atom A can be computed using Löwdin population analysis,

$$q_A = Z_A - \sum_{i \subset A} P_{ii}(t) \tag{4}$$

where Z_A is the charge on the nucleus, P_{ii} are the diagonal elements of the density matrix in the orthonormal basis, and the sum is over basis functions on atom A. Orbital occupation numbers can also be obtained by projecting the time-dependent density matrix onto the initial, field-free orbitals

$$n_k(t_i) = \mathbf{C}_k^T(0)\, \mathbf{P}(t_i)\, \mathbf{C}_k(0) \tag{5}$$

where $\mathbf{C}_k(0)$ is the kth eigenvector of the converged Fock matrix at $t = 0$. The instantaneous dipole moment is given by

$$\mu(t_i) = \sum_A Z_A \mathbf{R}_A - \mathrm{tr}(\mathbf{D}'\mathbf{P}'(t_i)) \tag{6}$$

where $\mathbf{D}'$ are the dipole moment integrals in the AO basis. For the purpose of analysis, it is also useful to write the components of the dipole in terms of the polarizability, α, and the first, second, and higher hyperpolarizabilities, β, γ, etc.

$$\mu_i = \mu_i^0 + \sum_j \alpha_{ij}E_j + \frac{1}{2}\sum_{jk}\beta_{ijk}E_jE_k + \frac{1}{6}\sum_{jkl}\gamma_{ijkl}E_jE_kE_l + \ldots \tag{7}$$

The β's are small or zero and do not contribute significantly for the polyenes in the present study.

Electronic dynamics in a field are simulated using the development version of the GAUSSIAN[59] series of programs with the addition of the modified midpoint unitary transform time-dependent Hartree−Fock algorithm (MMUT-TDHF). Calculations have been performed at the HF/6-31G(d,p) level of theory with a step size of 0.0012 fs (0.05 au). For each of the molecules, the integrations are carried out for 10 fs for CW fields and for 16 fs for pulsed fields. Field parameters are $|\mathbf{E}_{max}| = 0.05$ au (8.75×10^{13} W/cm^2) and $\omega = 0.06$ au (760 nm). The integrations were started from the converged electronic ground states. The phase of the field φ was chosen to be zero and the nuclei were not permitted to move during the calculation.

III. Results and Discussion

The TDHF simulations of ethylene, butadiene, and hexatriene +1 and +2 cations were carried out with simple fields as a first step to understanding the interaction of conjugated molecules with intense lasers. The effect of shaped pulses will be examined in subsequent investigations. Future studies of processes such as fragmentation and ionization will require more sophisticated methods.[52] The electronic dynamics of the molecules interacting with strong fields was monitored by examining the instantaneous dipole, the charge distribution, and orbital occupations with respect to the electric field. Instances when

the dipole moment or charges do not linearly respond to the field will be termed nonadiabatic behavior or response. A direct consequence of this is residual oscillations in the dipole moment and charge distribution after the field has returned to zero and these are considered diagnostic of nonadiabatic coupling or excitation. A quantitative estimate of adiabatic[60,61] response has been proposed for two level systems. In these systems the condition for adiabatic evolution is $\omega \ll \Delta_0^2/\epsilon_0$ were ω is the field frequency, Δ_0 is the field-free off-diagonal mixing term, and ϵ_0 are the field-free eigenvalues. The complexities of the multilevel systems studied here make such an elegant quantitative description very difficult. However, for trends in the polyene cation systems, nonlinearities in the response of the instantaneous dipole and the charges are sufficient for simple, qualitative assessments of nonadiabaticity. The response of each of the systems is simulated in both a CW laser field and a laser pulse lasting ca. 7 fs at a frequency corresponding to the commonly employed Ti:sapphire laser. For the first two cycles of the CW and the pulsed fields given by eqs 2 and 3, the response of each of the molecules considered in this paper is the same. The response at large times in the CW fields is already evident by the end of the second cycle. Because a pulsed field also lets us examine the behavior of the system after the field has returned to zero and to determine if there has been nonadiabatic coupling of the molecule to the field, it is a more versatile probe and is the focus of our discussion.

Figure 1 shows the geometries of the neutral, +1 cation, and +2 cation of ethylene, butadiene, and hexatriene, and their orientations with respect to the applied field. (At higher levels of theory ethylene monocation is twisted, but at the hartree-Fock level of theory it is planar.) Also shown in Figure 1 are the charge distributions (top, neutrals; middle, +1; bottom, +2) produced by a static field of 0.05 au. The adiabatic time-dependent response of a molecule to a laser field is governed by the low lying excited states and the relevant transition moments. For comparison with the nonadiabatic, full THDF simulations, Table 1 lists the lowest excitations for the polyene +1 and +2 cations at the neutral and optimized ion geometries calculated with the linear response TDHF method (also known as the random phase approximation (RPA)). Like the neutral molecules, the dications are closed shell systems and the lowest transition is dominated by the HOMO → LUMO excitation involving π orbitals (except for ethylene +2 cation, which has no π electrons). The monocations are open shell doublets and have lower lying excited states than the neutrals or the dications. The two lowest energy states for butadiene and hexatriene cation radical are linear combinations of excitations from the highest "doubly occupied" π orbital to the "singly occupied" π orbital (HOMO → SOMO) and from the "singly occupied" π orbital to the lowest unoccupied π^* orbital (SOMO → LUMO). As expected for the TDHF approximation, the calculated excitation energies for the +1 and +2 cations are 0.7−1.0 eV higher than the experimental values and recent MRMP2 calculations.[62]

For molecules without dipole moments, the polarizability is the leading term in the adiabatic response to an applied field, eq 7. The static and dynamic polarizabilities for ethylene, butadiene, and hexatriene neutral, monocation, and dication are collected in Table 2 for several levels of theory. For ethylene, there is very good agreement among the polarizabilities computed at various levels of theory with the same basis set and geometry. For the closed shell butadiene and hexatriene neutrals and dications, the Hartree−Fock polarizabilities are up to 20% higher than values obtained with PBE0 density functional theory and coupled cluster calculations with single and double excitations (CCSD) computed with the same basis set and geometry. For open shell butadiene and hexatriene monocation, the differences are about twice as large. The difference between the UHF and ROHF values indicates that most of this increase is due to spin contamination. However, the increase in polarizability is smaller than the differences between ethylene, butadiene, and hexatriene, and between the neutrals, monocations, and dications. The nonadiabatic effects may also be overestimated by a similar amount, but the trends

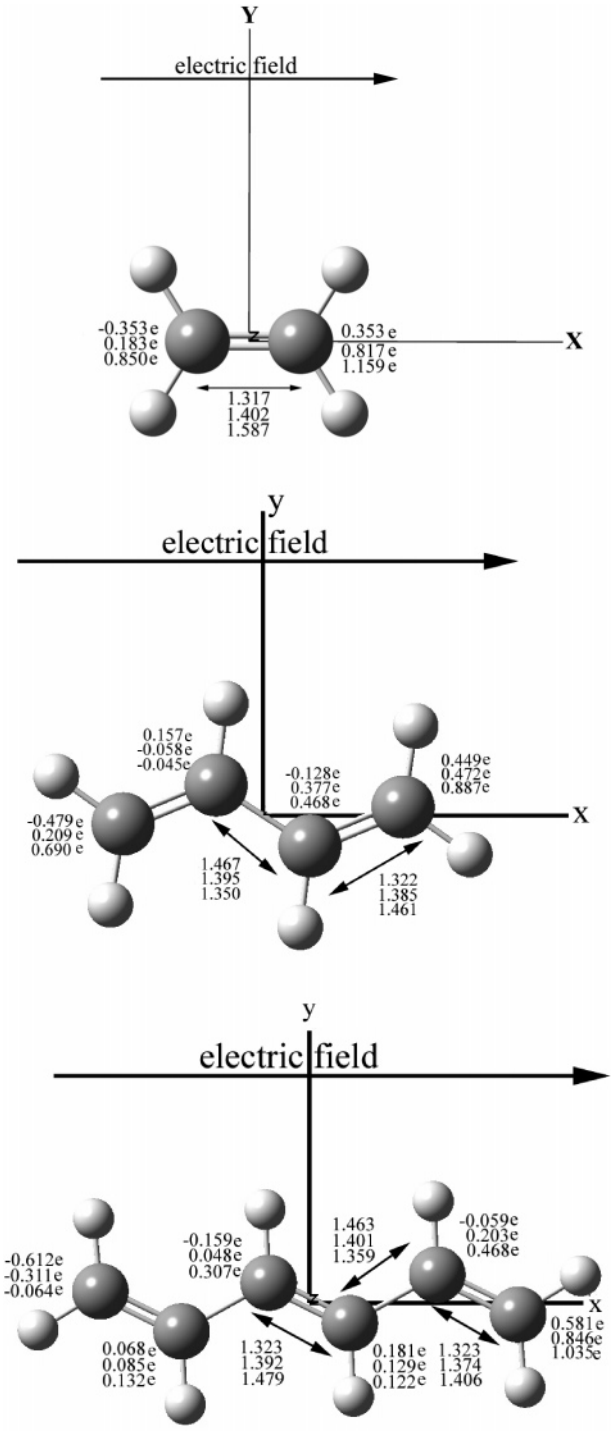

Figure 1. Ethylene, butadiene, and hextriene neutral, monocation, and dication computed at HF/6-31G(d,p), showing optimized bond lengths in the absence of a field and Löwdin charges on the CH and CH_2 groups in the presence of a 0.05 au field applied in the direction shown (top values for the neutral, middle values for the +1 cation, bottom values for the +2 cation).

TABLE 1: Lowest Vertical Excition Energies for Ethylene, Butadiene, and Hexatriene Cations with Linear Response TDHF/6-31G(d,p)[a]

main transitions (TDHF coefficient)	energy (eV) from TDHF	transition dipole moment	oscillator strength
Ethylene +1 Neutral Geometry			
SOMO → LUMO (0.99)	6.51	1.17	0.29
HOMO → LUMO + 3 (0.66)	16.29	1.51	0.92
HOMO − 1 → LUMO + 3 (0.70)	18.95	0.96	0.43
Ethylene +1 Ion Geometry			
SOMO → LUMO (0.99)	5.43	1.22	0.20
HOMO → LUMO + 3 (0.67)	16.35	1.48	0.88
HOMO − 1 → LUMO + 3 (0.58)	18.32	0.84	0.32
HOMO − 1 → LUMO + 5 (0.64)	21.56	0.95	0.47
Ethylene +2 Neutral Geometry			
HOMO → LUMO + 3 (0.70)	17.13	1.37	0.78
HOMO → LUMO + 6 (0.54)	20.93	1.51	1.17
HOMO − 2 → LUMO + 2 (0.61)	22.59	0.34	0.06
Ethylene +2 Ion Geometry			
HOMO − 1 → LUMO + 3 (0.66)	16.57	1.95	1.54
HOMO → LUMO + 5 (0.41)	18.43	0.89	0.36
HOMO − 1 → LUMO + 5 (0.68)	20.75	0.24	0.03
Butadiene +1 Neutral Geometry			
HOMO → SOMO (1.00)	2.53	1.70	0.12
SOMO → LUMO (0.92)	4.87	1.75	0.38
HOMO → LUMO + 1 (0.86)	10.43	0.58	0.11
Butadiene +1 Ion Geometry			
SOMO → LUMO (0.95)	4.03	1.94	0.39
HOMO → LUMO (0.83)	5.69	0.23	0.01
HOMO − 2 → LUMO + 1 (0.77)	8.79	0.11	0.01
Butadiene +2 Neutral Geometry			
HOMO → LUMO (0.71)	3.96	2.04	0.41
HOMO → LUMO + 2 (0.70)	11.51	0.16	0.18
Butadiene +2 Ion Geometry			
HOMO → LUMO (0.71)	4.83	0.96	0.44
HOMO − 2 → LUMO + 5 (0.45)	16.94	0.05	1.72
HOMO − 2 → LUMO + 7 (0.46)	19.11	0.06	0.68
Hexatriene +1 Neutral Geometry			
HOMO → SOMO (0.97)	2.74	2.56	0.45
SOMO → LUMO (0.89)	3.95	2.23	0.50
Hexatriene +1 Ion Geometry			
HOMO → SOMO (0.54)	3.04	3.52	0.93
SOMO → LUMO (0.59)	4.56	0.27	0.03
Hexatriene +2 Neutral Geometry			
HOMO → LUMO (0.70)	3.38	3.25	0.88
HOMO − 1→ LUMO + 1 (0.56)	9.42	0.40	0.07
HOMO → LUMO + 2 (0.50)	10.69	0.74	0.21
Hexatriene +2 Ion Geometry			
HOMO → LUMO (0.69)	4.38	2.98	0.95
HOMO − 1→ LUMO + 1 (0.60)	9.07	0.17	0.04
HOMO → LUMO + 2 (0.55)	10.49	0.05	0.17

[a] HOMO, highest occupied molecular orbital; SOMO, singly occupied molecular orbital; LUMO, lowest unoccupied molecular orbital.

should be correct. The modest differences between the ROHF and ROMP2 polarizabilities indicates that electron correlation plays only a minor role.

The calculation of the ionization rates is a complex issue for molecules. There have been several adjustments[26,27,63−65] to Ammosov−Delone−Krainov (ADK)[6] theory to make it more desirable for molecules with the most promising adjustment being MO-ADK[63] theory. MO-ADK theory has only been used for diatomic molecules. Extension of MO-ADK theory to the molecules of interest may be possible for future studies although the pulses used in these simulations are short enough that significant ionization should not take place.

A. Ethylene +1 Cation. The top panel of Figures 2 show the time evolution of the CW laser fields applied along the C═C axis of ethylene +1 cation. The second and third panels of Figures 2 show the response of the dipole moment and Löwdin charges for ethylene +1 cation at the neutral geometry. The instantaneous dipole and the charges appear to follow the field adiabatically. For the CW field of 0.05 au, the maximum in the instantaneous dipole moment is 1.27 au, whereas using eq 7 yields a dipole of 1.39 au for a field of 0.05 au and the dynamic polarizability calculated at the HF/6-31G(d,p) level of theory (Table 2, 27.80 au at $\omega = 0.06$ au). This can be compared with the adiabatic behavior of neutral ethylene for which the difference between the instantaneous dipole and eq 7 is only 0.4%. This suggests that there is already some nonadiabatic behavior in the monocation, even if not visible in the response of the charges and the dipole. Optimization of the geometry of the monocation leads to a lower excitation energy (Table 1, 5.34 eV vs 6.51 eV) and an increase in the polarizability (Table 2, 33.28 au). These changes are sufficient to make the nonadiabatic behavior much more apparent, as shown in panels 4 and 5 of Figure 2.

For the pulsed field in Figure 3a, the response of ethylene +1 cation is the same as the CW field for the first two cycles. After the field returns to zero, there are residual oscillations in the instantaneous dipole moment and the charges, indicating that the laser pulse has produced a small degree of electronic excitation or coupling. The oscillations are more pronounced for the optimized geometry of the cation. Fourier transformation of the residual oscillation of the dipole moment for the neutral geometry shows several peaks. The three largest peaks correspond to energies of 6.48, 16.20, and 18.97 eV. Table 1 indicates that these energies match the lowest $\pi \rightarrow \pi^*$ transition and higher energy $\sigma \rightarrow \sigma^*$ transitions calculated by linear response TDHF/6-31G(d,p) theory. For the cation optimized geometry (panel 4), the four largest peaks in the Fourier transform correspond to energies of 5.37, 16.34, 18.30, and 21.47 eV. Table 1 shows that these energies are the same transitions observed for the neutral geometry plus an additional higher lying $\sigma \rightarrow \sigma^*$ transition. In each instance of transition from ground to excited state, the energy of the excited state is lower for the optimized geometry and the height of the associated peak in the Fourier transform is greater. For example, the Fourier coefficient for the lowest $\pi \rightarrow \pi^*$ transition (5.37 eV) for the ion geometry is 19 times larger than the corresponding transition (6.48 eV) for the neutral geometry, in good agreement with the more pronounced oscillation of the ion optimized geometry dipole moment. Thus, the oscillation of the dipole moment is mainly associated with the lowest $\pi \rightarrow \pi^*$ transition; however, a few other higher energy transitions make a small contribution as well. This was also confirmed by examining the orbital occupation numbers, eq 6. Because the frequency of the electric field corresponds to an energy of 1.55 eV, these excitations must be associated with nonresonant, nonadiabatic processes. The amount of charge transfer obtained in the TDHF simulations is essentially the same as seen in a static field of the same magnitude (Figure 1).

B. Ethylene +2 Cation. The time evolution of ethylene +2 cation subject to a pulsed field is shown in Figure 3b. While the external field is present, the instantaneous dipole moment and charges follow the field adiabatically. For the neutral geometry, the maximum instantaneous dipole moment is 0.682 au, whereas the dipole moment calculated using eq 7 is 0.675 au, indicating that higher order processes are not important for the ethylene +2 cation at this field strength. The decrease in the maximum instantaneous dipole moment from the +1 to the +2 cation (1.281 vs 0.682 au) can be linked directly to the decrease in dynamic polarizability (27.80 vs 13.50 au, Table 2).

TABLE 2: Longitudinal Polarizabilities for Ethylene, Butadiene, Hexatriene and Their Cations[a]

	ethylene			butadiene			hexatriene		
	0	+1	+2	0	+1	+2	0	+1	+2
Neutral Optimized Geometry									
static α(0)									
UHF/6-31G(d,p)	32.71	27.10	13.35	79.72	129.09	86.39	151.72	269.92	215.62
ROHF/6-31G(d,p)	32.71	26.08	13.35	79.72	87.23	86.39	151.72	196.20	215.62
UPBE/6-31G(d,p)	30.88	26.45	13.69	77.51	83.47	75.06	153.66	184.38	184.63
ROMP2/6-31G(d,p)	29.00	25.06	13.35	69.12	94.25	67.05	129.60	189.25	183.43
UCCSD/6-31G(d,p)	29.10	27.96	13.38	68.24	93.12	71.71	124.96	200.41	204.52
dynamic α(ω)[b]									
UHF/6-31G(d,p)	32.88	27.80	13.50	81.69	178.5	98.87	154.5	347.2	269.5
UPBE0/6-31G(d,p)	31.11	24.41	14.03	78.09	96.58	84.01	157.1	257.8	222.3
Cation Optimized Geometry									
static α(0)									
UHF/6-31G(d,p)		31.58	17.30		114.47	71.35		274.78	157.08
ROHF/6-31G(d,p)		30.67	17.30		84.67	71.35		200.12	157.08
UPBE/6-31G(d,p)		26.04	17.37		83.51	70.56		187.04	158.05
ROMP2/6-31G(d,p)		25.71	17.23		92.17	74.69		193.46	158.66
UCCSD/6-31G(d,p)		27.46	17.26		92.93	71.46		194.98	161.40
dynamic α(ω)[b]									
UHF/6-31G(d,p)		33.28	17.44		133.5	76.85		366.3	175.8
UPBE0/6-31G(d,p)		26.82	17.52		90.75	79.42		218.3	179.2

[a] For the field directed along the long axis of the molecule as illustrated in Figure 1. [b] ω =760 nm.

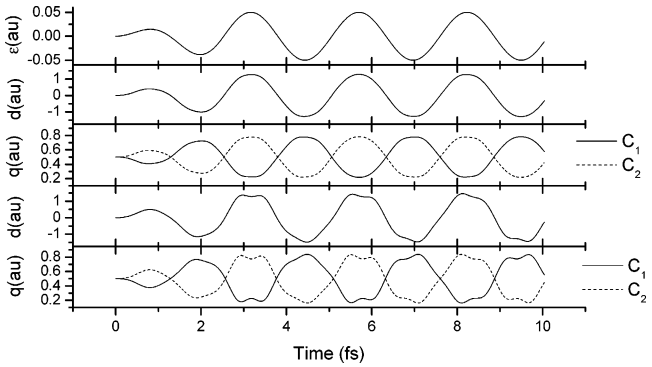

Figure 2. Time evolution of ethylene +1 in a CW field (TDHF/6-31G(d,p), $E_{max} = 0.05$ au (3.5×10^{14} W/cm^2) and $\omega = 0.06$ au (760 nm)), showing the electric field (top panel), instantaneous dipole and charge distribution for the neutral geometry (second and third panels), and the cation optimized geometry (fourth and fifth panels).

After the field has returned to zero, there are some very small residual oscillations of the dipole moment and the charges. These oscillations are orders of magnitude smaller than for the +1 cation. The Fourier transform of the dipole moment oscillation shows the three largest peaks correspond to energies of 17.13, 20.84, and 22.69 eV for the neutral geometry and 16.57, 18.41, and 20.71 eV for the ion geometry. Comparison with Table 1 shows that these agree well with energies calculated at the linear response TDHF/6-31G(d,p) level of theory and correspond to excitations which are $\sigma \rightarrow \sigma^*$ transitions.

C. Butadiene +1 Cation. The orientation of butadiene +1 in the field is shown in Figure 1 and the response of the charge distribution is presented in Figure 4a. In contrast to ethylene, the dipole does not follow the field adiabatically and the charges show significant nonadiabatic behavior. In particular, the charges on C_1 and C_4 oscillate several times before the phase changes with the field, and the charges on C_2 and C_3 respond quite erratically. The charge transfer between the two halves of the molecule (0.58 electron) is considerably larger than that seen in a static field (see Figure 1). The maximum magnitude of the instantaneous dipole is 4.09 au in the TDHF simulations. In accord with the strong nonadiabatic behavior, this is quite different from the value of 8.93 au obtained from eq 7.

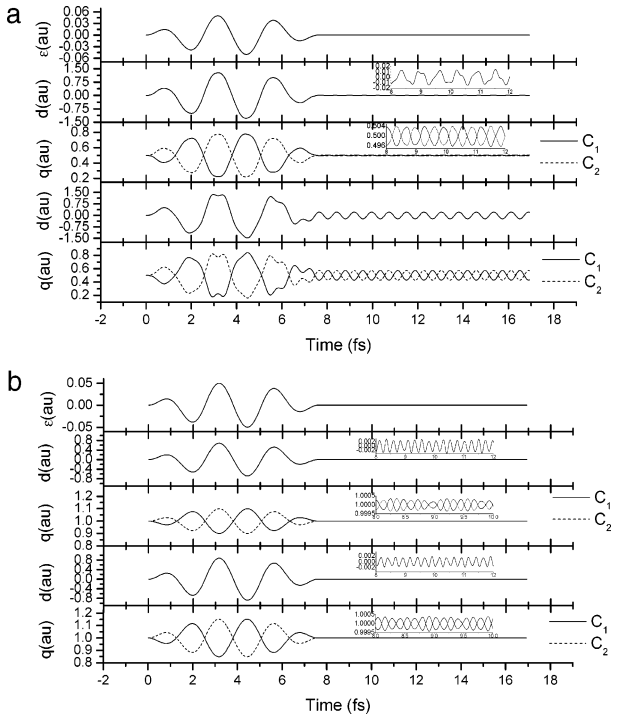

Figure 3. Time evolution of (a) ethylene +1 and (b) ethylene +2 in a pulsed field (TDHF/6-31G(d,p), $E_{max} = 0.05$ au (3.5×10^{14} W/cm^2) and $\omega = 0.06$ au (760 nm)), showing the electric field (top panel), instantaneous dipole and charge distribution for the neutral geometry (second and third panels), and the cation optimized geometry (fourth and fifth panels).

The oscillation of the dipole moment after the field returns to zero is complex at both geometries so Fourier transform analysis was used to determine the underlying frequency components. For the neutral geometry, the Fourier transform contains several peaks and the largest ones correspond to energies of 2.57 and 4.90 eV. Table 1 shows that these are associated with the HOMO $\rightarrow$ SOMO and SOMO $\rightarrow$ LUMO transitions which are the lowest lying π type transitions. Other smaller peaks correspond to higher $\pi \rightarrow \pi^*$ transitions or differences between excited states. Analysis for the ion optimized geometry again shows several peaks with the largest

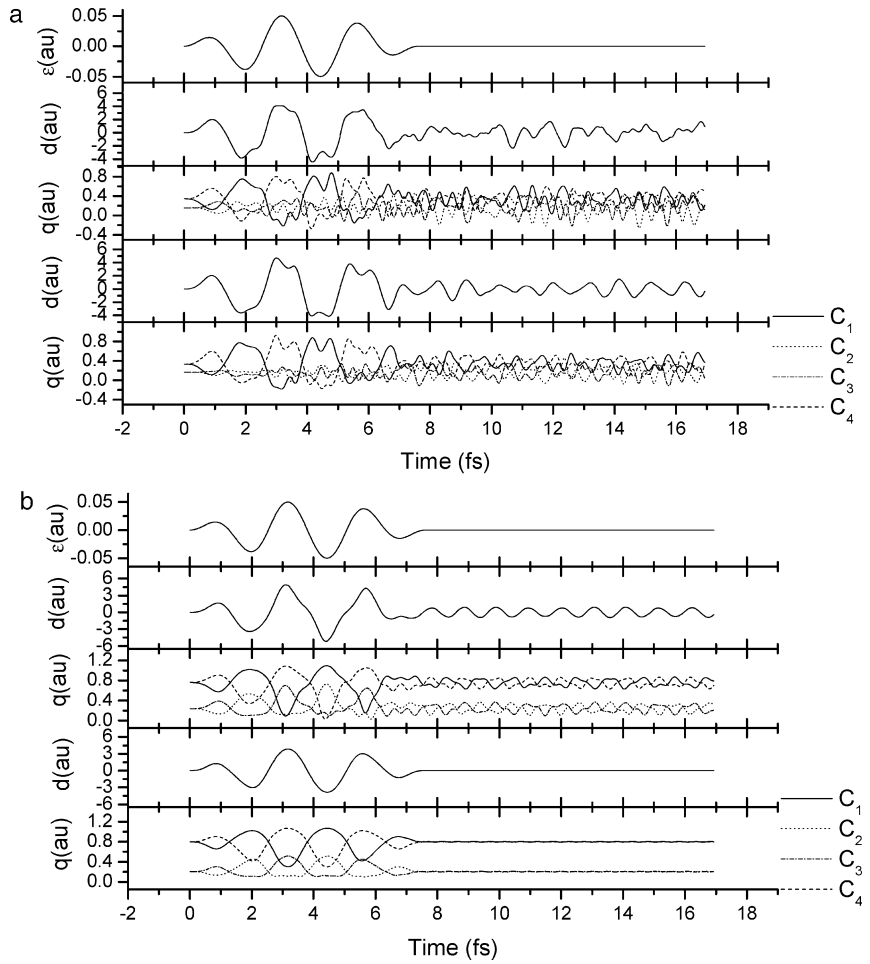

Figure 4. Time evolution of (a) butadiene +1 and (b) butadiene +2 in a pulsed field (TDHF/6-31G(d,p), $E_{max} = 0.05$ au (3.5×10^{14} W/cm^2) and $\omega = 0.06$ au (760 nm)), showing the electric field (top panel), instantaneous dipole and charge distribution for the neutral geometry (second and third panels), and the cation optimized geometry (fourth and fifth panels).

peaks corresponding to energies of 4.10 and 5.69 eV. The first two excited states correspond to the SOMO → LUMO and HOMO → LUMO transitions (see Table 1). The lower excited-state energies and higher oscillator strengths at the neutral geometry than at the ion geometry, account for the larger dynamic polarizability at the neutral geometry. For the neutral geometry, the two peak heights for the HOMO → SOMO and SOMO → LUMO are almost the same, leading to a more complex pattern for the dipole oscillation. The dipole moment oscillations at the optimized geometry are dominated by one frequency and consequently more periodic. The oscillations of the charges after the field is off are also quite large and complex. In fact, the magnitudes of the charge oscillations after the field returns to zero are 0.3−0.4 times the magnitude with the field on. The Fourier analysis of the dipole, the charge oscillations and the orbital occupancies (not shown) all suggest that the significant electron coupling was produced by the pulse.

D. Butadiene +2 Cation. As can be seen from Figure 4b, the dipole moment response of the dication is more adiabatic than that of the monocation. The response of the charges is significantly more complex than for the neutral (see Figure 4a of ref 41), but not as complex as the monocation. This is in good agreement with the fact that the dynamic polarizability for butadiene +2 is somewhat larger than that for the neutral but is much smaller than that for monocation (see Table 2). The oscillations of the dipole moment after the field returns to zero are much more periodic than for butadiene +1 and their magnitude is smaller. The energies of the main peaks in the Fourier transform of the dipole moment correspond to energies of 3.94 eV for the neutral geometry and 4.78 eV for the ion geometry. Table 1 shows that for both geometries, the lowest energy is associated with the HOMO → LUMO transition, which is the lowest energy π transition. The peak height in the Fourier transform corresponding to this transition is 75 times larger for the neutral geometry than the ion optimized geometry. There are a number of smaller peaks for both geometries related to various $\pi \rightarrow \pi^*$ and $\sigma \rightarrow \sigma^*$ transitions (see Table 1). The larger oscillations seen for butadiene at the neutral geometry may be attributable to the fact that the excitation energy is lower for the neutral geometry than for +2 cation with the optimized geometry.

E. Hexatriene +1 Cation. The response of the dipole and charge distribution of hexatriene +1 to the pulsed field is shown in Figure 5a. The nonadiabatic behavior of the instantaneous dipole and the charges is readily apparent in a number of aspects. Although the charges on C_1 and C_6 for hexatriene +1 do change sign when the field changes sign, they oscillate between sign changes. The charge response of carbons C_2, C_3, C_4, and C_5 is very complicated. The charges change sign several times during a field cycle and their amplitudes are comparable. The degree of charge transfer between the two halves of the molecule (0.89 electron) is larger than in butadiene +1 cation and larger than in a static field (Figure 1). In the TDHF simulations, the instantaneous dipole has a maximum magnitude of 10.72 au. By comparison, using eq 7 yields a dipole of 17.36 au. This indicates that there is a large nonadiabatic contribution to the

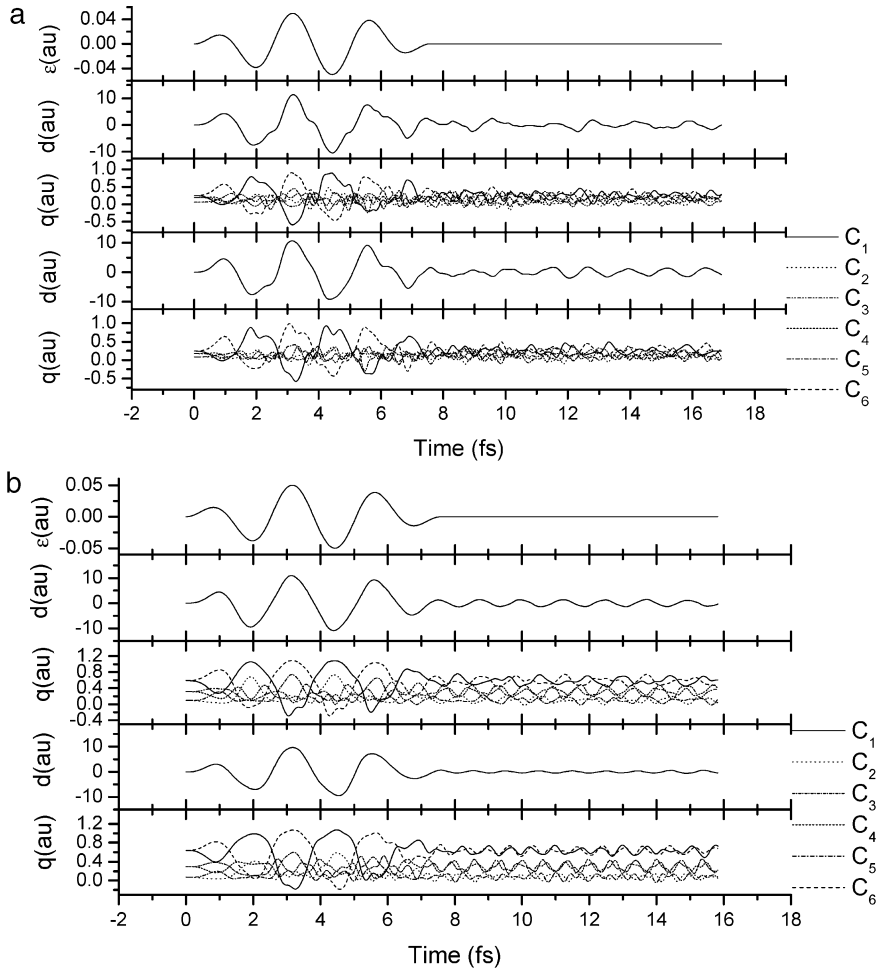

Figure 5. Hexatriene +1 and (b) hexatriene +2 in a pulsed field (TDHF/6-31G(d,p), $E_{max} = 0.05$ au (3.5×10^{14} W/cm^2) and $\omega = 0.06$ au (760 nm)), showing the electric field (top panel), instantaneous dipole and charge distribution for the neutral geometry (second and third panels), and the cation optimized geometry (fourth and fifth panels).

dipole response. The instantaneous dipole continues to oscillate after the field is turned off; however, the oscillations are again complex. The Fourier transform of the residual dipole moment shows peaks corresponding to energies of 2.81 and 3.99 eV for the neutral geometry and 3.07 and 4.48 eV for the ion geometry. As for butadiene +1, the first two excitation energies for both geometries correspond to HOMO → SOMO and SOMO → LUMO transitions, which are again the lowest lying π type transitions (see Table 1). There are also low energy peaks in the Fourier transform that correspond to the difference between excited-state energies and some higher energy peaks that correspond to the sum of excited-state energies. The peak heights in the Fourier transform for the HOMO → SOMO and SOMO → LUMO transitions for both geometries follow the pattern exhibited by butadiene +1. For the neutral geometry, the peak heights for the two lowest frequencies are similar. The dipole moment oscillation for the ion geometry is dominated by one frequency in the Fourier transform and consequently the response is smoother.

F. Hexatriene +2 Cation. The evolution of the dipole moment and charges are shown in Figure 5b for hexatriene +2 cation. The response of the dipole moment is more adiabatic than for hexatriene +1, but the charges still show complex and nonadiabatic behavior. The maximum magnitude of the dipole moment is 10.92 au compared to 13.42 au using eq 7. This suggests nonadiabatic effects contribute significantly to the response of the dipole moment. The dipole moment again shows oscillations after the field has returned to zero. In the Fourier transforms of the dipole oscillations for each geometry, the lowest energy excitation corresponds to the HOMO → LUMO π type transition and the peak height in the Fourier transform for the neutral geometry 3 times as large as for the ion geometry. This agrees well with the dipole oscillation amplitudes in Figure 5b. Thus, the oscillations of the dipole moment after the field returns to zero are due to nonadiabatic coupling and excitation of the lowest π type transition at each geometry.

IV. Conclusion

In this paper, we have used TDHF to simulate strong laser fields interacting with a series of polyene cations of increasing length and conjugation. The +1 and +2 cations of ethylene, butadiene, and hexatriene were examined after ionization with the field aligned along the long axis of the molecules and a laser intensity of 8.75×10^{13} W/cm^2 and wavelength of 760 nm. The time evolution of the charges, instantaneous dipole, and orbital occupation numbers were used to assess the effect of strong fields on these polyenes. As in the case of the neutral molecules, not only the π electrons but also the lower lying σ orbitals respond to the strong field. The monocations of butadiene and hexatriene display very pronounced nonadiabatic effects. For the same laser intensity, nonadiabatic effects increase with the length of the polyene for a given charge state and geometry. The effects are larger for the monocations than for the dications or the neutrals. For different charge states of a given molecule, polarizability may be an indicator of adiabatic

versus nonadiabatic behavior. For pulsed fields, the instantaneous dipole continues to oscillate after the field is off. The dipole oscillations after the field returns to zero are very complex for the +1 cations of butadiene and hexatriene whereas they are more periodic for the rest of the cations. These simulations indicate that nonadiabatic excitation of polyatomic molecules by a nonresonance strong-field laser pulse is possible. Fourier analysis of the oscillations of the instantaneous dipole shows that the nonresonant electronic excitation involved the lowest electronic transition. For a particular molecule and charge state, the degree of nonadiabatic excitation was larger for geometries with lower excitation energies. This indicates that future studies should include the effect of molecular motion as well as electron dynamics in the study of molecules in strong fields.

Acknowledgment. This work was supported by the National Science Foundation (CHE 0512144, H.B.S. and CHE 313967, R.J.L.), and Gaussian, Inc.

References and Notes

(1) Assion, A.; Baumert, T.; Bergt, M.; Brixner, T.; Kiefer, B.; Seyfried, V.; Strehle, M.; Gerber, G. *Science* **1998**, *282*, 919.
(2) Levis, R. J.; Menkir, G. M.; Rabitz, H. *Science* **2001**, *292*, 709.
(3) DeWitt, M. J.; Levis, R. J. *Phys. Rev. Lett.* **1998**, *81*, 5101.
(4) Levis, R. J.; DeWitt, M. J. *J. Phys. Chem. A* **1999**, *103*, 6493.
(5) Keldysh, L. V. *Sov. Phys. JTEP* **1965**, *20*, 1307.
(6) Ammosov, M. V.; Delone, N. B.; Krainov, V. P. *JTEP* **1986**, *81*, 5101.
(7) Eberly, J. H.; Javanainen, J.; Rzazewski, K. *Phys. Rep.* **1991**, *204*, 331.
(8) Bucksbaum, P. H.; Zavriyev, A.; Muller, H. G.; Schumacher, D. W. *Phys. Rev. Lett.* **1990**, *64*, 1883.
(9) Nandor, M. J.; Walker, M. A.; Van Woerkom, L. D.; Muller, H. G. *Phys. Rev. A* **1999**, *60*, R1771.
(10) Zuo, T.; Bandrauk, A. D. *J. Nonlin. Opt. Phys. Mater.* **1995**, *4*, 533.
(11) McPherson, A.; Gibson, G.; Jara, H.; Johann, U.; Luk, T. S.; McIntyre, I. A.; Boyer, K.; Rhodes, C. K. *J. Opt. Soc. Am.* **1987**, *4*, 595.
(12) Lhuillier, A.; Schafer, K. J.; Kulander, K. C. *J. Phys. B* **1991**, *24*, 3315.
(13) Antoine, P.; Lhuillier, A.; Lewenstein, M. *Phys. Rev. Lett.* **1996**, *77*, 1234.
(14) Salieres, P.; Antoine, P.; de Bohan, A.; Lewenstein, M. *Phys. Rev. Lett.* **1998**, *81*, 5544.
(15) Lezius, M.; Blanchet, V.; Rayner, D. M.; Villeneuve, D. M.; Stolow, A.; Ivanov, M. Y. *Phys. Rev. Lett.* **2001**, *86*, 51.
(16) Lezius, M.; Blanchet, V.; Ivanov, M. Y.; Stolow, A. *J. Chem. Phys.* **2002**, *117*, 1575.
(17) Markevitch, A. N.; Smith, S. M.; Romanov, D. A.; Schlegel, H. B.; Ivanov, M. Y.; Levis, R. J. *Phys. Rev. A* **2003**, *68*, 011402(R).
(18) Markevitch, A. N.; Romanov, D. A.; Smith, S. M.; Schlegel, H. B.; Ivanov, M. Y.; Levis, R. J. *Phys. Rev. A* **2004**, *69*, 013401.
(19) Zavriyev, A.; Bucksbaum, P. H.; Muller, H. G.; Schumacher, D. W. *Phys. Rev. A* **1990**, *42*, 5500.
(20) Frasinski, L. J.; Posthumus, J. H.; Plumridge, J.; Codling, K.; Taday, P. F.; Langley, A. J. *Phys. Rev. Lett.* **1999**, *83*, 3625.
(21) Zuo, T.; Bandrauk, A. D. *Phys. Rev. A* **1995**, *52*, R2511.
(22) Cornaggia, C.; Lavancier, J.; Normand, D.; Morellec, J.; Agostini, P.; Chambaret, J. P.; Antonetti, A. *Phys. Rev. A* **1991**, *44*, 4499.
(23) Cornaggia, C.; Schmidt, M.; Normand, D. *J. Phys. B* **1994**, *27*, L123.
(24) Bhardwaj, V. R.; Corkum, P. B.; Rayner, D. M. *Phys. Rev. Lett.* **2003**, *91*, art. no. 203004.
(25) Markevitch, A. N.; Romanov, D. A.; Smith, S. M.; Levis, R. J. *Phys. Rev. Lett.* **2004**, *92*, art. no. 063001.
(26) DeWitt, M. J.; Levis, R. J. *J. Chem. Phys.* **1998**, *108*, 7739.
(27) DeWitt, M. J.; Levis, R. J. *J. Chem. Phys.* **1999**, *110*, 11368.
(28) Tchaplyguine, M.; Hoffmann, K.; Duhr, O.; Hohmann, H.; Korn, G.; Rottke, H.; Wittmann, M.; Hertel, I. V.; Campbell, E. E. B. *J. Chem. Phys.* **2000**, *112*, 2781.
(29) von Helden, G.; Holleman, I.; Knippels, G. M. H.; van der Meer, A. F. G.; Meijer, G. *Phys. Rev. Lett.* **1997**, *79*, 5234.
(30) Muth-Bohm, J.; Becker, A.; Chin, S. L.; Faisal, F. H. M. *Chem. Phys. Lett.* **2001**, *337*, 313.
(31) Schulz, M.; Tretiak, S.; Chernyak, V.; Mukamel, S. *J. Am. Chem. Soc.* **2000**, *122*, 452.
(32) Tretiak, S.; Chernyak, V.; Mukamel, S. *Phys. Rev. Lett.* **1996**, *77*, 4656.
(33) Tretiak, S.; Chernyak, V.; Mukamel, S. *Chem. Phys. Lett.* **1996**, *259*, 55.
(34) Meier, T.; Mukamel, S. *Phys. Rev. Lett.* **1996**, *77*, 3471.
(35) Shanker, B.; Applequist, J. *J. Phys. Chem.* **1996**, *100*, 10834.
(36) Chen, G. H.; Mukamel, S. *J. Phys. Chem.* **1996**, *100*, 11080.
(37) Kirtman, B.; Toto, J. L.; Robins, K. A.; Hasan, M. *J. Chem. Phys.* **1995**, *102*, 5350.
(38) Smith, S. M.; Markevitch, A. N.; Romanov, D. A.; Li, X. S.; Levis, R. J.; Schlegel, H. B. *J. Phys. Chem. A* **2004**, *108*, 11063.
(39) Ingamells, V. E.; Papadopoulos, M. G.; Raptis, S. G. *Chem. Phys. Lett.* **1999**, *307*, 484.
(40) Rozyczko, P. B.; Bartlett, R. J. *J. Chem. Phys.* **1998**, *108*, 7988.
(41) Oliveira, L. N.; Amaral, O. A. V.; Castro, M. A.; Fonseca, T. L. *Chem. Phys.* **2003**, *289*, 221.
(42) Smith, S. M.; Li, X. S.; Markevitch, A. N.; Romanov, D. A.; Levis, R. J.; Schlegel, H. B. *J. Phys Chem A* **2005**, *109*, 5176.
(43) Harumiya, K.; Kono, H.; Fujimura, Y.; Kawata, I.; Bandrauk, A. D. *Phys. Rev. A* **2002**, *66*, art. no. 043403.
(44) Kawata, I.; Bandrauk, A. D.; Kono, H.; Fujimura, Y. *Laser Phys.* **2001**, *11*, 188.
(45) Lein, M.; Kreibich, T.; Gross, E. K. U.; Engel, V. *Phys. Rev. A* **2002**, *65*, art. no. 033403.
(46) Yu, H. T.; Zuo, T.; Bandrauk, A. D. *Phys. Rev. A* **1996**, *54*, 3290.
(47) Talebpour, A.; Vijayalakshmi, K.; Bandrauk, A. D.; Nguyen-Dang, T. T.; Chin, S. L. *Phys. Rev. A*, **2000**, *6204*, art. no. 042708.
(48) Suzuki, M.; Mukamel, S. *J. Chem. Phys.* **2003**, *119*, 4722.
(49) Suzuki, M.; Mukamel, S. *J. Chem. Phys.* **2004**, *120*, 669.
(50) Hankin, S. M.; Villeneuve, D. M.; Corkum, P. B.; Rayner, D. M. *Phys. Rev. Lett.* **2000**, *84*, 5082.
(51) Hankin, S. M.; Villeneuve, D. M.; Corkum, P. B.; Rayner, D. M. *Phys. Rev.* **2001**, *6401*, art. no. 013405.
(52) Li, X. S.; Tully, J. C.; Schlegel, H. B. *J. Chem. Phys.* **2005**, *123*, 084106.
(53) Li, X. S.; Smith, S. M.; Markevitch, A. N.; Romanov, D. A.; Levis, R. J.; Schlegel, H. B. *Phys. Chem. Chem. Phys.* **2005**, *7*, 233.
(54) Kulander, K. C. *Phys. Rev. A* **1987**, *36*, 2726.
(55) Kulander, K. C. *Phys. Rev. A* **1987**, *35*, 445.
(56) Tsiper, E. V.; Chernyak, V.; Tretiak, S.; Mukamel, S. *Chem. Phys. Lett.* **1999**, *302*, 77.
(57) Micha, D. A. *J. Phys. Chem. A* **1999**, *103*, 7562.
(58) Micha, D. A. Density matrix treatment of electronic rearrangement. In *Adv. Quantum Chem.* **1999**, *35*, 317.
(59) Frisch, M. J.; Trucks, G. W.; Schlegel, H. B.; Scuseria, G. E.; Robb, M. A.; Cheeseman, J. R.; Montgomery, J. A., Jr.; Vreven, T.; Kudin, K. N.; Burant, J. C.; Millam, J. M.; Iyengar, S. S.; Tomasi, J.; Barone, V.; Mennucci, B.; Cossi, M.; Scalmani, G.; Rega, N.; Petersson, G. A.; Nakatsuji, H.; Hada, M.; Ehara, M.; Toyota, K.; Fukuda, R.; Hasegawa, J.; Ishida, M.; Nakajima, T.; Honda, Y.; Kitao, O.; Nakai, H.; Klene, M.; Li, X.; Knox, J. E.; Hratchian, H. P.; Cross, J. B.; Bakken, V.; Adamo, C.; Jaramillo, J.; Gomperts, R.; Stratmann, R. E.; Yazyev, O.; Austin, A. J.; Cammi, R.; Pomelli, C.; Ochterski, J. W.; Ayala, P. Y.; Morokuma, K.; Voth, G. A.; Salvador, P.; Dannenberg, J. J.; Zakrzewski, V. G.; Dapprich, S.; Daniels, A. D.; Strain, M. C.; Farkas, O.; Malick, D. K.; Rabuck, A. D.; Raghavachari, K.; Foresman, J. B.; Ortiz, J. V.; Cui, Q.; Baboul, A. G.; Clifford, S.; Cioslowski, J.; Stefanov, B. B.; Liu, G.; Liashenko, A.; Piskorz, P.; Komaromi, I.; Martin, R. L.; Fox, D. J.; Keith, T.; Al-Laham, M. A.; Peng, C. Y.; Nanayakkara, A.; Challacombe, M.; Gill, P. M. W.; Johnson, B.; Chen, W.; Wong, M. W.; Gonzalez, C.; Pople, J. A. *Gaussian 03*, development version; Gaussian, Inc.: Wallingford, CT, 2004.
(60) McCann, J. F.; Bandrauk, A. D. *Phys. Lett. A* **1990**, *151*, 509.
(61) Kayanuma, Y. *Phys. Rev. A* **1997**, *55*, R2495.
(62) Kawashima, Y.; Nakayama, K.; Nakano, H.; Hirao, K. *Chem. Phys. Lett.* **1997**, *267*, 82.
(63) Tong, X. M.; Zhao, Z. X.; Lin, C. D. *Phys. Rev. A* **2002**, *66*, art. no. 033402.
(64) Tong, X. M.; Zhao, Z. X.; Lin, C. D. *J. Mod. Opt.* **2005**, *52*, 185.
(65) DeWitt, M. J.; Levis, R. J. *J. Chem. Phys.* **1998**, *108*, 7045.